RSC Advances

PAPER

View Article Online
View Journal | View Issue

Cite this: *RSC Adv.*, 2023, **13**, 2780

In situ synthesis of polythiophene encapsulated 2D hexagonal boron nitride nanocomposite based electrochemical transducer for detection of 5-fluorouracil with high selectivity†

Magesh Kumar Muthukumaran, Muthukumar Govindaraj, Bharathi Kannan Raja and Arockia Selvi J *

It is difficult for the scientific community to develop a nonenzymatic sensing platform for extremely sensitive and selective detection of specific biomolecules, antibiotics, food adulterants, heavy metals, *etc.* One of the most significant chemotherapy drugs, 5-fluorouracil (5-Fu), which is used to treat solid malignancies, has a fluorine atom in the fifth position of the uracil molecule. Recognizing the secure and effective dosing of drugs for chemotherapy continues to be a critical concern in cancer disease management. The maintenance of the optimal 5-Fu concentration is dependent on the presence of 5-Fu in biofluids. Herein we reported a conducting polymer encapsulated 2D material, PTh/h-BN for the efficient electrochemical detection of anticancer drug 5-Fu. Furthermore, the synthesized PTh/h-BN nanocomposite was confirmed by the High-Resolution Transmission Electron Microscope (HR-TEM), High-Resolution Scanning Electron Microscope (HR-SEM), X-ray diffraction (XRD), and Fourier-Transform Infrared Spectroscopy (FT-IR). The electrical resistance of PTh/h-BN modified GCE and its sensing performance towards 5-Fu were tested using Electrochemical Impedance Spectroscopy (EIS) and Cyclic Voltammetry (CV) studies respectively. The analytical performance of our proposed catalyst was tested using Differential Pulse Voltammetry (DPV), and the amperometry (*i*–*t* curve) method. From the results, our proposed PTh/h-BN nanocomposite-modified GCE shows enhanced sensing performance due to higher redox peak currents, large active surface area, and high electrical conductivity. Moreover, the nanohybrid shows enhanced sensing performances with quick response time, wide linear range, the lowest limit of detection, high sensitivity, and high selectivity in the presence of various interferents. Finally, the practical applicability of the proposed sensor was tested with real-world samples with very good recovery percentages.

Received 11th November 2022
Accepted 5th January 2023

DOI: 10.1039/d2ra07147a

rsc.li/rsc-advances

1. Introduction

The increased use of anticancer medication in various medical sectors is indispensable, however, the side effects caused due to its usage prompted the development of sensors for anticancer drugs. Concerning the crucial biological aspects, the pharmacological specificity of these medications is quite important.[1] 5-Fluorouracil (5-Fu) is an anticancer drug used to treat various types of cancers such as colon, esophageal, stomach, pancreatic, breast, and cervical cancer.[2] However, 5-Fu is toxic to the gastrointestinal system and bone marrow cells when injected exceeding the standard dosage form.[3,4] Despite its widespread use in chemotherapy, 5-Fu's limited absorption is a serious drawback in clinical practice.[5] Thereby, frequent concentration measurements of 5-Fu are necessary to keep an adequate level of the drug in physiological fluids. However, an overdose of 5-Fu, accumulates in cancer patients which could be highly toxic. Cancer cells are similar to normal human cells.[6] Despite, the danger of serious side effects due to 5-Fu's, non-specificity makes its detection in biological fluids, a topic of great interest in oncologic therapy.[7] Hence, regulating the quantity of 5-Fu in a particular formulation with a preferred dosage is essential to ensure drug quality control and clinical diagnosis. So, a quick, reliable, and very selective performance analysis approach was developed for samples commonly used anticancer drugs (5-fluorouracil).[4] In addition, intracellular 5-Fu metabolites can cause cell death by inhibiting thymidylate synthase or by incorporating into RNA and DNA,[8] both of which trigger apoptosis.[9–11]

As a result, advanced analytical approaches for sensitive 5-Fu concentration monitoring in pharmaceuticals and biological samples are still being developed.[12] For instance, methods such as HPLC Analysis,[13] fluorescence,[14] electrochemical sensors,[15]

Department of Chemistry, SRM Institute of Science and Technology, Kattankulathur, 603203, Tamil Nadu, India. E-mail: arockiaj@srmist.edu.in; arockiaselvi29@yahoo.co.in

† Electronic supplementary information (ESI) available. See DOI: https://doi.org/10.1039/d2ra07147a

AAS,[16] and chromatography methods[17] are used for the detection of 5-Fu at its concentration level. Regardless the approaches of previously discussed, electrochemical sensing has been identified as one of the best methods for quick response, greater sensitivity, selectivity, low cost, ease to handle, *etc.*[18] Moreover, the electrochemical sensing method has proven to be the most sensitive method to detect various analytes such as biomolecules (glucose,[19] ascorbic acid,[20] H_2O_2,[21] uric acid,[22] *etc.*), pharmaceutical substances (paracetamol,[23] dopamine,[24] chloramphenicol,[25] *etc.*), and food additives (colouring agents,[26] flavonoids,[27] preservatives,[28] *etc.*), heavy metals,[29] *etc.* In future, the electrochemical sensors have several appealing analytical properties and are viable candidates for clinical diagnostics.[30]

Recently two-dimensional materials are widely used for various applications such as supercapacitors,[31] HER,[32] OER,[33] ORR,[34] and electrochemical sensors[35] due to their enormous electro and physiochemical properties, atomic thinness, more specific surface area, and more responsive to the surface interactions.[36] According to that, hexagonal boron nitride is a recently sparked 2D material similar to graphite, within the layer, electron-deficient boron atoms, and electron-rich nitrogen atoms are alternatively bound by strong covalent bonds, whereas the layers are held together by weak van der Waals forces giving a layered structure.[37,38] The electrical conductivity was improved by increasing the electrochemical active surface area by successful liquid phase exfoliation, and surface functionalization.[36,39,40] As an organic part of Conducting Polymers (CPs) such as polyaniline (PANI), polythiophene (PTh), and polypyrrole (PPy) are of great interest due to their unique physical and chemical properties such as adjustable architecture, adaptability, charge carrier channeling, versatility, high thermal, chemical stability, and enormous electrical conductivity.[41–44] Most interestingly, polythiophene (PTh) is a conducting polymer with a low band gap of 2 eV as it has an electron-rich sulfur atom.[45] Moreover, the PTh is adorned on the top of the 2D h-BN nanosheets, further improving the sensing performance with high precision and accuracy due to the high electrical conductivity,[46] conjugated electronic system in the structure of the PTh,[47] enhanced the activity of h-BN after functionalization.[47,48]

Herein, for the first time, we reported a simple PTh/h-BN nanocomposite was synthesized by the *in situ* polymerization method, and the proposed electrocatalyst was successfully used for 5-Fu electrochemical detection. The highly conductive sulfur-containing polymer (PTh) network accelerates the electron transportation towards the h-BN nanosheets to achieve enhanced electrochemical sensing performances and most significantly.

2. Experimental section

2.1. Materials and methods

All the chemicals and reagents [thiophene monomer (C_4H_4S) (≥99% SRL), ferric chloride ($FeCl_3$) (≥98% AR), boron nitride bulk (h-BN) (≥99% SRL), sodium hydroxide (NaOH) (≥98% FISHER), acetonitrile, ethanol, methanol, 5-fluorouracil ($C_4H_3FN_2O_2$) (≥99% SRL), uric acid ($C_5H_4N_4O_3$) (≥99% SRL), lactose ($C_{12}H_{22}O_{11}$) (≥98% SRL), oxalic acid (≥99.5% AR), ascorbic acid ($C_6H_8O_6$) (≥99.7% SRL), dopamine ($C_8H_{11}NO_2$) (≥99% SRL), L-cysteine ($C_3H_7NO_2S$) (≥99% SRL), glucose ($C_6H_{12}O_6$) (≥99% SRL), potassium ferricyanide ($C_6N_6FeK_3$) (≥99% SRL), potassium ferrocyanide ($C_6FeK_4N_6$) (≥99% SRL), potassium chloride (KCl) (99.8% Fisher), monosodium hydrogen phosphate (NaH_2PO_4) (≥99% SRL), and disodium hydrogen phosphate (Na_2HPO_4) (≥99% SRL)] are purchased in Sigma Aldrich and Alfa Aesar. To create a stock solution, ultrapure deionized water was used. NaH_2PO_4 and Na_2HPO_4 were combined to create 0.1 M phosphate buffer (PBS) (pH = 7.0) for the detection of 5-Fu. The human blood serum sample was collected from SRM Medical College Hospital and Research Center, Kattankulathur, Tamil Nadu, for real sample analysis. All the experiments were done by using Milli-Q-water (18.2 MΩ cm @ 25 ± 2 °C).

2.2. Materials characterization

High-resolution scanning electron microscopy (HR-SEM, Thermoscientific Apreo S) and transmission electron microscopy (TEM, JEM-2100 Plus, JEOL) were utilized to predict the morphological, surface properties, and chemical content, and the selected area electron diffraction (SAED) pattern of produced h-BN, and PTh/h-BN hybrid. Energy dispersive spectroscopy (EDS-JEM-2100 Plus, JEOL, and Thermoscientific Apreo S) was utilized for elemental and chemical composition. The crystalline nature of the synthesized compound was examined by using X-ray diffraction spectroscopy (XRD system-X'pert powder, with Cu-Kα radiation (λ = 0.154 nm) Malvern Panalytical, United Kingdom) at 45 kV (tension) and 40 mA (current) with 0.02° per step scan and 1° per min speed. The functional groups of the synthesized materials were analyzed by Fourier Transform Infrared Spectroscopy (FT-IR) technique, (FT-IR spectrophotometer, Shimadzu, IR Tracer 100). The cyclic voltammetry (CV), electrochemical impedance spectroscopy (EIS), differential pulse voltammetry (DPV), and amperometry (*i–t* curve) studies were carried out using CHI electrochemical workstation (CHI 760E, USA). All the measurements were performed at room temperature using a three-electrode setup. The counter, reference, and working electrodes were platinum wire (Pt), Ag/AgCl (3 M KCl), and glassy carbon electrode (GCE), respectively.

2.3. Synthesis of polythiophene

A previously published conventional chemical oxidation procedure was used to synthesize polythiophene (PTh)[49,50] (Scheme 1). The PTh was synthesized in a three-necked round bottom flask containing dichloromethane in 0.5 M thiophene monomer. A freshly prepared anhydrous $FeCl_3$ solution in acetonitrile (1 : 3 molar ratio of monomer : $FeCl_3$) was added dropwise to the above reaction mixture under vigorous stirring (1200 rpm) for 24 hours at room temperature. At the end of the reaction, a yellow solution turns into a dark brown precipitate, confirming the formation of polythiophene. The obtained product was centrifuged and washed with distilled water and ethanol several times to remove the unreacted particles and impurities. Finally, the obtained powder was collected and dried at 60 °C in a vacuum oven for 14 hours.

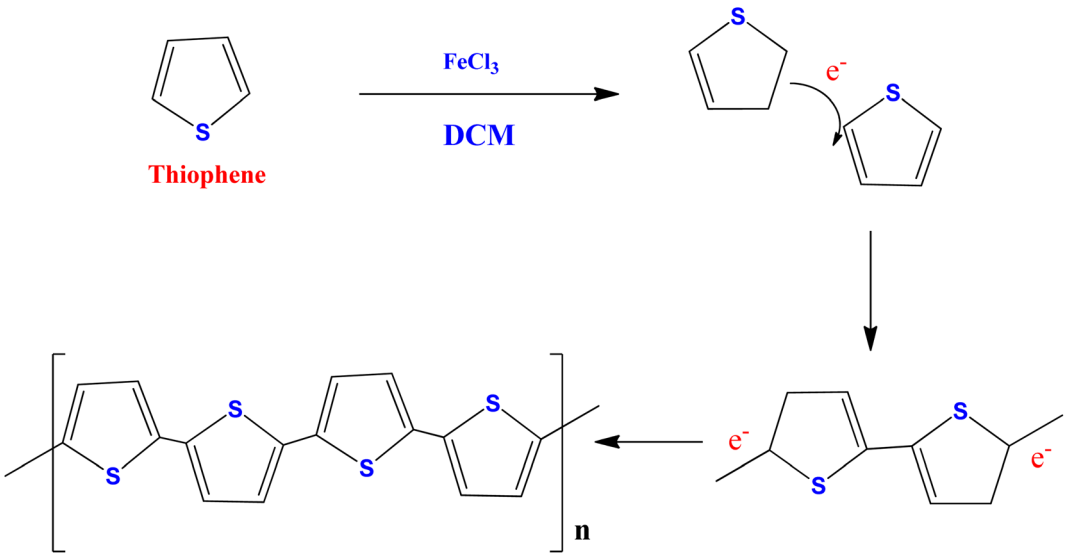

Scheme 1 Polymerization mechanism of thiophene monomer.

2.4. Liquid-phase exfoliation of h-BN

To obtain boron nitride nanosheets (BNNS), 500 mg of the pristine h-BN is dispersed in 10 mL of PBS (pH = 7) was exfoliated using bath-sonication for 30 minutes, followed by ultra-probe sonication for 3 hours (3 s ON/2 s OFF and 54 percent amplitude). After that, the dispersion was centrifuged at 3000 rpm for 30 minutes and the top 70 percent of the floatable BN dispersion was collected, further, the floatable solution was again centrifuged at 8000 rpm for 15 minutes. The obtained powder was dispersed in 10 mL of distilled water added and bath sonicated for 30 minutes to re-disperse them several times to remove the undesirable ions.[51,52]

2.5. Synthesis of PTh/h-BN nanocomposite

The PTh/h-BN nanocomposite was synthesized using single-step *in situ* polymerization.[41] First, to make h-BN nanosheets, 0.1 g of h-BN was dispersed in 20 mL of ethanol and ultra-sonicated for 1 hour, and a prepared thiophene monomer in dichloromethane was added dropwise under constant stirring to make a homogeneous suspension. Further, the freshly prepared $FeCl_3$ was added dropwise to the reaction mixture under vigorous stirring at room temperature for 24 hours. Upon the addition of $FeCl_3$ was initiated the polymerization process and the colour changed to pale brown which confirms the development of PTh/h-BN composite. The achieved outcome was collected and centrifuged and rinsed with distilled water and followed by ethanol several times to remove the unreacted particles and impurities. Finally, the obtained pale brown precipitate was dried at 50 °C for 12 hours (Scheme 2).

2.6. Electrode fabrication

The glassy carbon electrode (GCE) was shining with an 0.5 M alumina slurry, ultra-sonicated with H_2O and ethanol before electrode modification. Finally, the polished GCE was rinsed with DI water before being dried in a hot air oven at 60 °C. After which, 8 μL of composite dispersion was dropped on the GCE surface and dried for 10 minutes at 60 °C (Scheme 3).

2.7. Preparation of real sample

The practical feasibility of PTh/h-BN/GCE was investigated using human blood serum samples which were further centrifuged at 6000 rpm for 10 minutes and filtered *via* a Whatman filter paper to remove undesirable contaminants before the electrochemical analyses. The human blood serum samples were then tested after being diluted with 0.1 M PBS solution (pH = 7.0).

3. Results and discussion

3.1. XRD and FT-IR analysis

The crystal clear of the synthesized substances was analyzed by X-ray diffraction (XRD) pattern. Fig. 1(A) shows the XRD pattern of pure PTh (a), h-BN (b), and PTh/h-BN (c) nanocomposite. The XRD spectrum of PTh (Fig. 1(A) curve a) reveals the material is amorphous in nature, with a broad peak at 21–28° which corresponds to plane (001) is a good agreement and it shows less percentage of crystallinity.[53] Followed by, the XRD spectrum of h-BN shows a characteristic peak at 26.25°, 41.6°, 43.8°, 55.1°, and 75.5° could be attributed to crystalline planes (002), (100), (101), (004) and (110) respectively and the results are well matched with the (JCPDS card number 34-0421)[54] shown in Fig. 1(A) curve b. Further, the PTh/h-BN nanocomposite was shown in Fig. 1(A) (curve c), the characteristic peaks produced by h-BN are seen with low peak intensity, and diffraction peaks slightly shifted due to the successful exfoliation of h-BN and the formation of PTh/h-BN nanocomposite. Conversely, all the individual diffraction peaks were observed in the PTh/h-BN hybrid, which revealed the successful preparation of the composite.

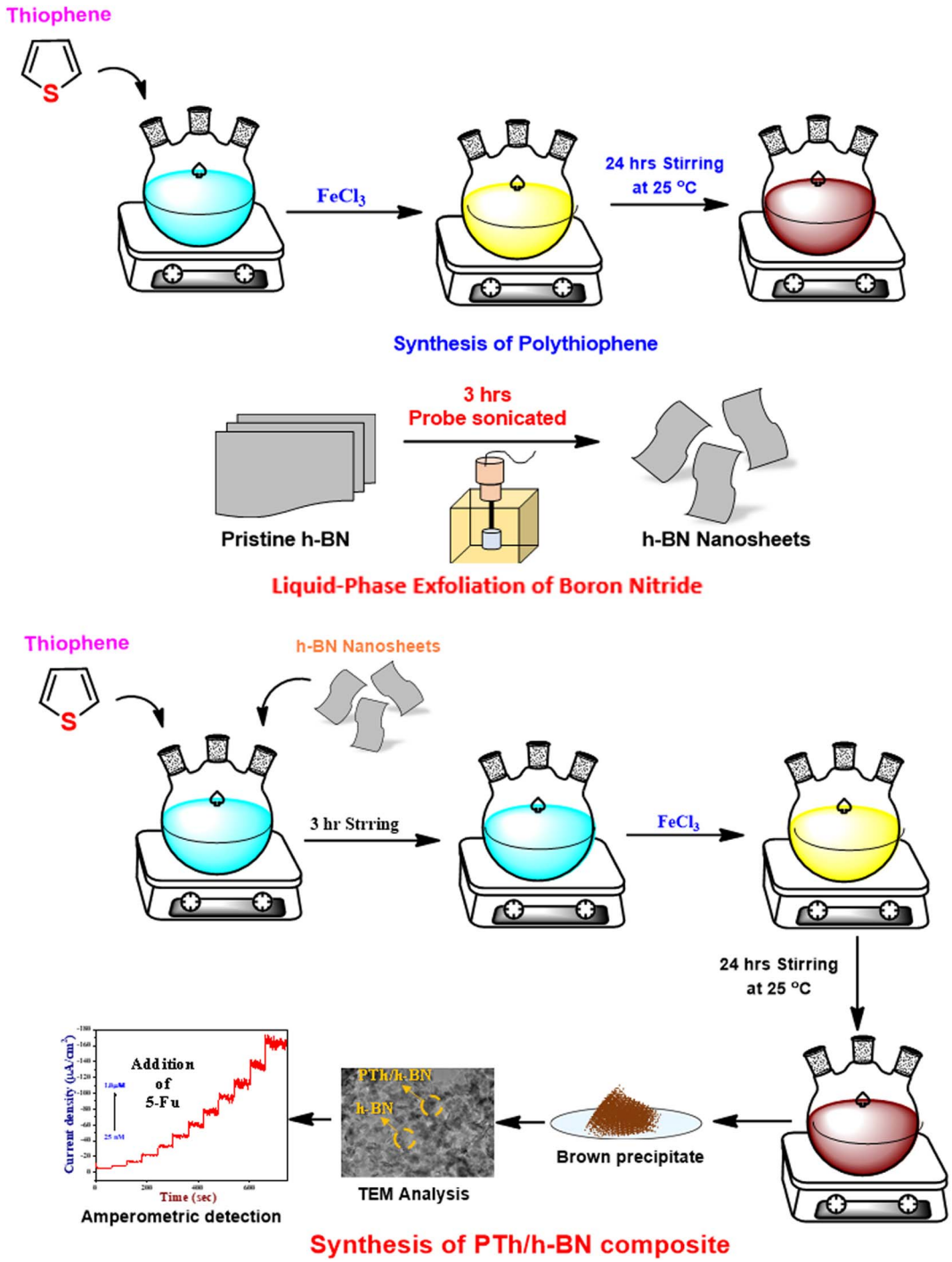

Scheme 2 Synthesis of PTh, h-BN and PTh/h-BN nanocomposite.

Next, the functional groups present in the synthesized PTh, h-BN, and PTh/h-BN hybrid was analyzed by Fourier transform infrared spectroscopy (FT-IR) as shown in Fig. 1(B). The PTh spectrum was showing the transmittance peaks at ~632 cm^{-1} (C–S stretching), 1187 cm^{-1} (C–H out of plane bending), ~1676 cm^{-1} (C=C stretching), ~2571 to 2938 cm^{-1} (C–H stretching vibrations) which is shown in Fig. 1(B) curve a.[49,55] Additionally, Fig. 1(B) curve b shows the FT-IR spectrum of h-BN, showing several absorption bands at ~786 cm^{-1} (B–N stretching), ~1280 cm^{-1} (B–N–B bending), corresponding to in-plane BN stretching vibration of sp^2-bonded h-BN and out of plane B–N–B bending vibration, respectively.[56,57] Furthermore, the peak at ~3312 cm^{-1} (hydroxyl) indicates the hydroxylation of h-BN nanosheets. Moreover, the FT-IR spectrum of PTh/h-BN nanocomposite (Fig. 1(B) curve c) exhibited various absorption peaks at ~655 cm^{-1} (C–S–C bending), ~766 cm^{-1} (B–N bending), ~877 cm^{-1} (C–H), ~1352 cm^{-1} (B–N Stretching), ~1613 cm^{-1} (C=H) and ~3218 cm^{-1} (O–H stretching).

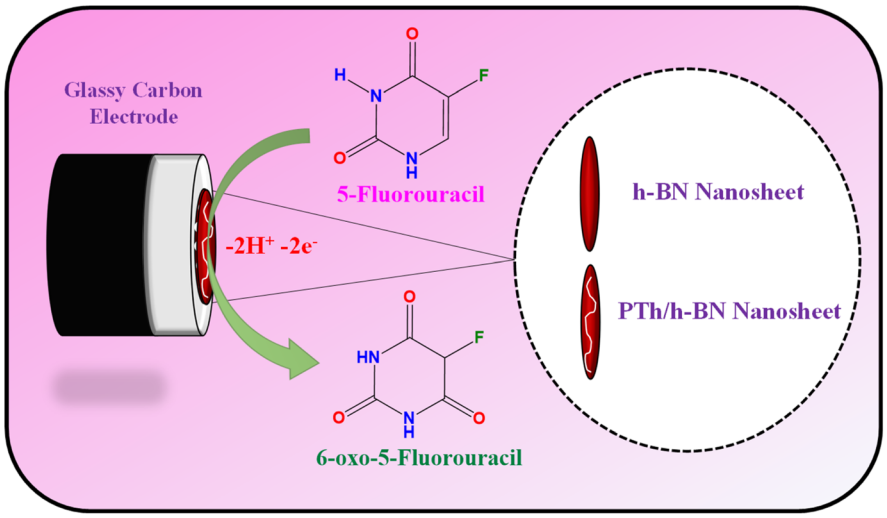

Scheme 3 Graphical representation of the electrode fabrication and oxidation of 5-Fu towards PTh/h-BN/GCE.

However, the peak weakening and shift to the shorter wavenumbers shows the successful formation of PTh on the exterior of the h-BN nanosheets denotes a change in the chemical environment that occurred during composite formation. The presence of PTh and h-BN in the PTh/h-BN hybrids as well as their successful combination are thus revealed by the FT-IR results.

3.2. Surface morphology analysis

The surface morphology and structure of the synthesized PTh, h-BN, and PTh/h-BN composite were examined utilizing HR-SEM and HR-TEM analysis (Fig. 2). Furthermore, morphological structures of the generated PTh, h-BN, and PTh/h-BN hybrid materials reveal the linkage between the PTh, and h-BN composite showed in SEM Analysis. Fig. 2(A–C), shows the surface structure of the PTh (A), h-BN (B), and PTh/h-BN (C) composite. Fig. 2(A) It is evident from these data that the polymerization process of thiophene produced polythiophene with an ordered structure, which was accountable for the increased electrical conductivity.[58] Fig. 2(B) shows the structure of the h-BN nanosheets seen that the exfoliation of the h-BN nanosheet from h-BN pristine and noted that the nanosheets having a high surface area should advantage for the electrochemical and biosensors. Fig. 2(C) shows the morphology study of the PTh/h-BN composite confirms the PTh is encapsulated on the exterior of the h-BN nanosheets in the form of chain

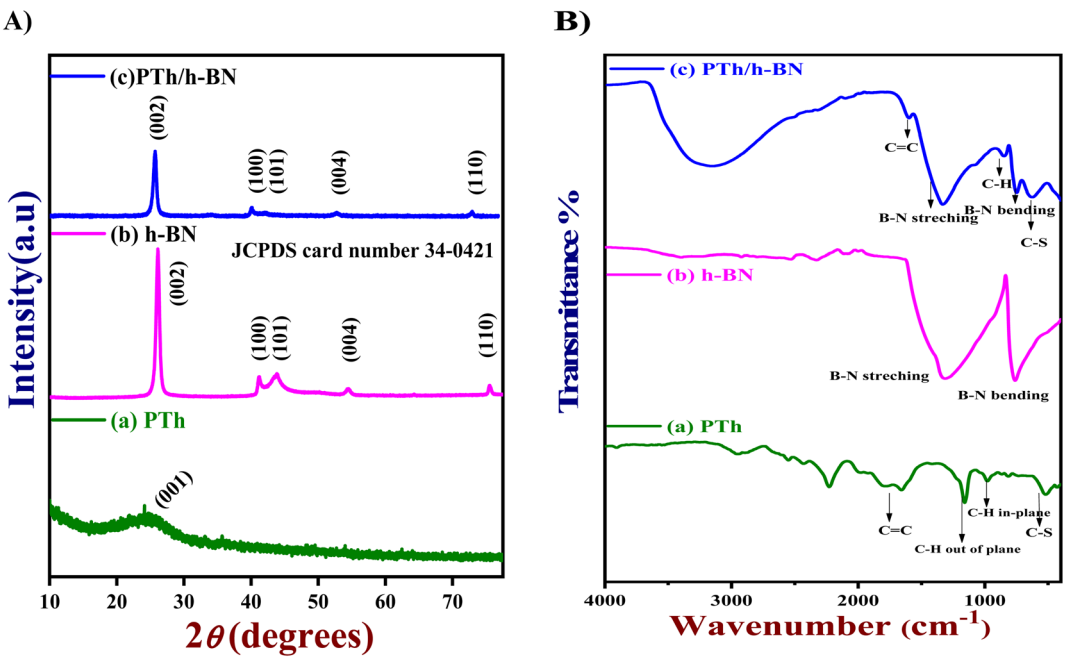

Fig. 1 (A) XRD patterns and (B) FT-IR spectra of (a) PTh, (b) h-BN, and (c) PTh/h-BN composite, respectively.

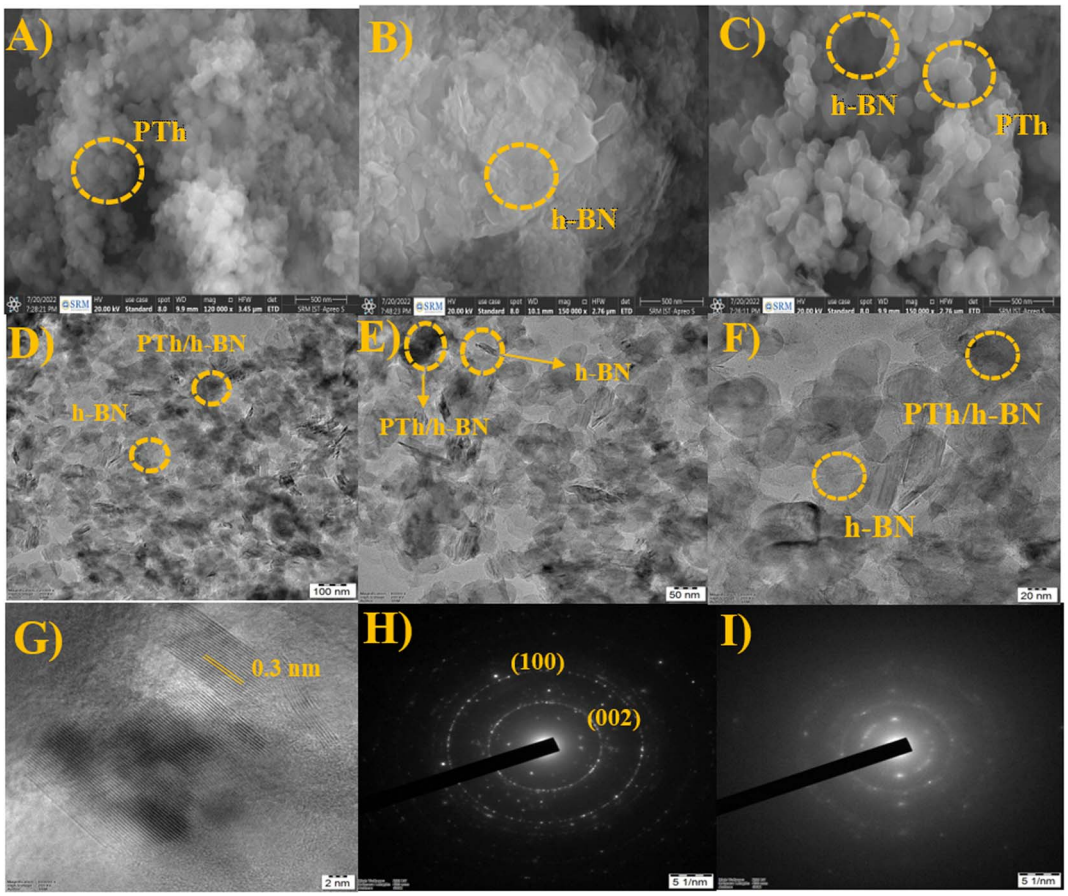

Fig. 2 (A–C) SEM images of PTh, h-BN, and PTh/h-BN composite, (D–F) TEM images and (G) lattice fringes of PTh/h-BN composite, (H and I) SAED pattern of h-BN and PTh/h-BN composite.

formation on the top of the h-BN nanosheet surface. However, PTh having a delocalized pi-electron is responsible for enhancing the conductivity in the PTh/h-BN composite. In addition, energy-dispersion spectroscopy (EDS) was used to confirm the respective elements (in atomic percentages) of B, N, C, O, and S in the PTh, h-BN, and PTh/h-BN composite. Moreover, the distribution of all elements in each compound, such as PTh (Fig. S_1†), h-BN (Fig. S_2†), and PTh/h-BN (Fig. S_3†) composite was validated by the HR-SEM-EDS elemental mapping pictures.

Additionally, using HR-TEM, the structure, and composition of PTh/h-BN composite was investigated. The TEM image of PTh demonstrated the successful construction of a polymer structure and the TEM image of h-BN demonstrated the formation of nanosheets as stacking flat layers in Fig. 2(D–F). The lattice fringes of PTh/h-BN composite was shown in Fig. 2(G). The dark shades indicate the amorphous nature of PTh encapsulated on the top of the h-BN nanosheets. The PTh/h-BN hybrid was successfully obtained according to the findings, which were in strong agreement with the HR-SEM findings and found the selected-area electron diffraction pattern of h-BN and PTh/h-BN composite in Fig. 2(H) and (I). The h-BN crystal planes (002), (100) and amorphous nature of PTh of broad peak plane (001) corresponding selected-area electron diffraction pattern could be seen clearly in Fig. 2(H) and (I). According to the HR-TEM results, PTh was successfully decorated on the surface of the h-BN nanosheets and confirmed the XRD findings, which showed that adding more active sites increased the specific surface area of the produced material, increasing its electrocatalytic activity.

3.3. Electrochemical properties

In order to understand the kinetic barrier and electron transfer process at the solid–liquid interface, the electrocatalytic activity of bare GCE, PTh, h-BN and PTh/h-BN modified GCE was tested at 50 mV s^{-1} in 0.1 M KCl which contains 5 mM $K_3[Fe(CN)_6]$ and $K_4[Fe(CN)_6]$ in the potential range between −0.3 V to 0.6 V *vs.* Ag/AgCl. Although, the observed anodic and cathodic peak potentials (E_{pa} & E_{pc}), oxidation and cathodic peak current densities (J_{pa} & J_{pc}), and the difference in potential (ΔE_p) were compared and listed in Table 1. Furthermore, the redox peaks for the redox reaction of $[Fe(CN)_6]^{3-/4-}$ which were observed in the bare GCE, PTh, h-BN, PTh/h-BN modified GCE were shown in Fig. 3(A). In comparison to the other electrodes, PTh/h-BN/GCE has a maximum anodic & cathodic current (I_p) and a lower peak-to-peak potential separation (E_p). Due to the higher surface area of the PTh/h-BN hybrid that offers the acceptable metal–solution interface for the accretion of charges or ions and

Table 1 CV profiles of the various modified and their potentials, resistivities, and current values in 0.1 M KCl containing 5 mM $[Fe(CN)_6]^{3-/4-}$ at a scan rate of 50 mV s^{-1}

Sl. no.	Modified electrodes	E_{pa} (V)	E_{pc} (V)	ΔE_p (mV)	J_{pa} (mA cm^{-2})	J_{pc} (mA cm^{-2})	R_{ct} (ohm)
1	Bare GCE	0.290	0.014	276	−0.820	0.745	130.19
2	PTh/GCE	0.219	0.059	160	−0.974	0.990	103.73
3	h-BN/GCE	0.246	0.062	184	−1.018	1.067	106.90
4	PTh/h-BN/GCE	0.217	0.078	139	−1.128	1.158	99.67

strengthens the fast electron transferability which is the primary factor for the maximum redox current response of PTh/h-BN/GCE during electro-catalysis. So, the conductivity of the composite material of PTh/h-BN/GCE is higher compared to PTh/GCE and h-BN/GCE, and the ΔE_p was attained to be 276, 184, 160, and 139 mV for bare GCE, h-BN, PTh, and PTh/h-BN modified GCE, respectively. The smaller value of ΔE_p with the magnificent I_{pa} at the PTh/h-BN/GCE specifies the quick electron transfer.

To examine the electrode activity of the electrochemical process to determine the dielectric properties of materials and electrochemical impedance spectroscopy (EIS)[59] was taken and analyzed by Nyquist plot of unmodified GCE, PTh, h-BN, and PTh/h-BN modified GCE in 0.1 M KCl that contains 5 mM $K_3[Fe(CN)_6]$ and $K_4[Fe(CN)_6]$. At a high frequency, Nyquist plots show a characteristic semi-circular curve at the electrode/solution contact. In EIS spectra, a semicircle obtained at a higher frequency corresponds to electron-transfer resistance (R_{ct})[60] and a semicircle obtained at a lower frequency describes electron diffusion. This experiment was carried out in the frequency range from 10 Hz to 600 Hz at a constant amplitude of 50 mV and the Nyquist curve of unmodified GCE, PTh/GCE, h-BN/GCE, and PTh/h-BN/GCE is shown in Fig. 3(B). Besides, the semicircle diameter of the bare/GCE is greater due to the high resistance and the R_{ct} value was found to be 130.19 Ω. The R_{ct} value of PTh/GCE was 103.73 Ω, the h-BN/GCE was 106.90 Ω

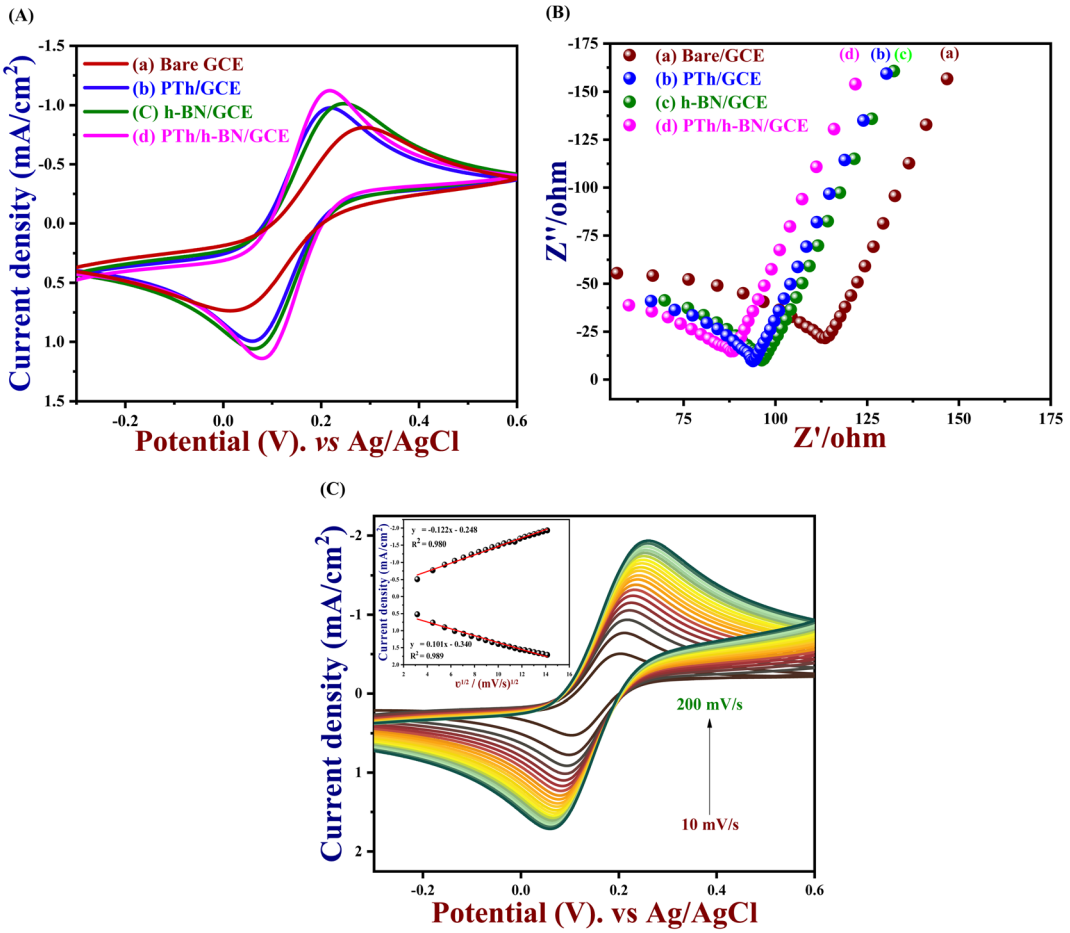

Fig. 3 (A) CV and (B) EIS response of bare/GCE (a), PTh/GCE (b), h-BN/GCE (c), and PTh/h-BN/GCE (d) in 0.1 M KCl with 5 mM $[Fe(CN)_6]^{3-/4-}$ at a scan rate of 50 mV s^{-1}, (C) CVs of the PTh/h-BN/GCE in 0.1 M KCl with 5 mM $[Fe(CN)_6]^{3-/4-}$ at an increasing scan rate of 10–200 mV s^{-1}.

and the PTh/h-BN/GCE had a very low resistance of 99.67 Ω which suggests that there was fast electron transfer between the electrode surface and the supporting electrolyte.

And performing the different scan rates from 10 to 200 mV s^{-1} in cyclic voltammetry indicates that the increase in scan rate will show a change in peak potential as shown in Fig. 3(C). Due to the sluggish electron transfer rate constant, the anodic and cathodic peak current defers linearly, and even peak separation increases, because it requires high potentials to cause electron transfer. The electrochemically active surface area of all the modified electrodes and the unmodified electrode was measured by the following eqn (1).

$$I_p = 2.69 \times 10^5 A n^{3/2} C D^{1/2} \nu^{1/2} \quad (1)$$

where 'I_p' represents peak current, 'n' represents the number of electrons involved in the chemical reaction, 'A' represents the surface area of the modified electrode, and 'C' represents the concentration of $[Fe(CN)_6]^{4-/3-}$ in bulk solution (5 mM), '$\nu^{1/2}$' is the square root of scan rate, '$D^{1/2}$' is the square root of diffusion coefficient. The active surface area was calculated as 0.077, 0.087, 0.094, and 0.112 cm^2 for unmodified GCE, PTh/GCE, h-BN/GCE, and PTh/h-BN/GCE, respectively. The following eqn (2) was used to compute the rates of charge transfer coefficient (K_s) of bare GCE, PTh/GCE, h-BN/GCE, and PTh/h-BN/GCE.

$$R_{ct} = \frac{RT}{n^2 F^2 K_s C} \quad (2)$$

where 'K_s' stands for the charge transfer rate, 'C' stands for a $[Fe(CN)_6]^{4-/3-}$ concentration, 'n' stands for the number of electrons, and 'R, T, and F' represent their typical meanings.[61,62] The rate constant (K_s) value of PTh/h-BN/GCE was determined to be 5.25×10^{-7} cm s^{-1}, indicating that PTh/h-BN/GCE has a higher catalytic activity than other modified and unmodified electrodes such as bare GCE (4.02×10^{-7} cm s^{-1}), h-BN/GCE (4.89×10^{-7} cm s^{-1}), and PTh/GCE (5.04×10^{-7} cm s^{-1}). At last, the above electrical characteristic results confirmed that the PTh/h-BN/GCE composite possesses a high active surface and possesses higher current density, quicker electron transfer, lower ΔE_p, and higher charge transfer rate than h-BN/GCE and PTh/GCE.

3.4. Electrochemical performance of 5-fu using PTh/h-BN nanocomposite

The electrochemical performance of 5-Fu towards the bare electrode, PTh, h-BN, and PTh/h-BN modified GCE was investigated in 0.1 M PBS (pH 7.0) at 50 mV s^{-1} by using cyclic voltammetry technique. Fig. 4(A) (inset) illustrates the CV curves of modified and unmodified electrodes in the absence of 5-Fu and initially, there was no oxidation peak observed on the surface of bare GCE and PTh/h-BN electrodes (Fig. 4(A) inset curves (a) and (b)). After the addition of 5-Fu (50 μM) (Fig. 4(A) curve a), a poor oxidation peak on the bare GCE surface at a potential of +1.20 V with a lower oxidation current density of −11.40 μA cm^{-2} due to the bad active surface area for electron transfer and less availability of electrocatalytic active sites. Followed by the bare GCE surface with the modification of PTh and h-BN for the sensing of 5-Fu, whereas the oxidation potential was observed at +1.14 V and +1.15 V with an oxidation current density of −31.26 μA cm^{-2} and -31.26 μA cm^{-2} shown this in Fig. 4(A) curves b and c. Interestingly, compared with the other electrodes, PTh/h-BN hybrid modified GCE showed a lower oxidation potential of +1.10 V with a higher current density of −46.98 μA cm^{-2} towards the 5-Fu detection (Fig. 4(A) curve d).

The enormous sensing capability of the PTh/h-BN/GCE is due to the quick electron transfer, large surface area, and the layered structure which accelerates the oxidation of 5-Fu (Scheme 4).[63] The 5-fluorouracil is electrochemically oxidized to 6-oxo-5-fluorouracil at a potential of +1.05 V at the surface of the modified electrodes with the removal of two electrons and two protons. The π–π bond of h-BN allows the electric charge carrier to travel freely in the entire lattice, which improves the speed of electron transport and PTh having functional group (sulfur) as

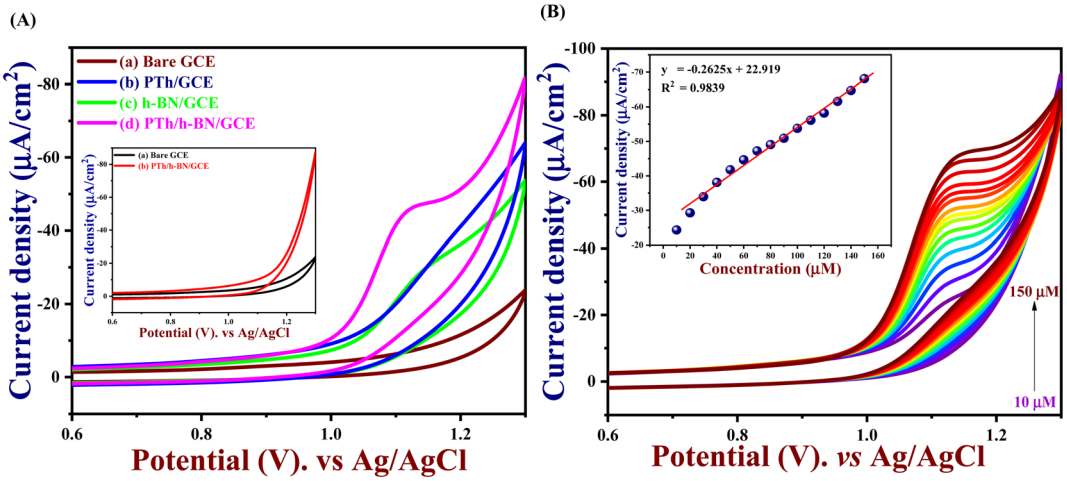

Fig. 4 (A) CV studies of bare/GCE (a), PTh/GCE (b), h-BN/GCE (c), and PTh/h-BN/GCE (d) in presence of 50 μM 5-Fu in 0.1 M PBS at a scan rate of 50 mV s^{-1} (inset: CV studies of bare/GCE (a), and PTh/h-BN/GCE (b) in the absence of 5-Fu in 0.1 M PBS), (B) CV profiles of PTh/h-BN/GCE in 0.1 M PBS (pH 7.0) containing 5-Fu (10–150 μM) (inset: linear plot between the concentration of the 5-Fu *vs.* current density).

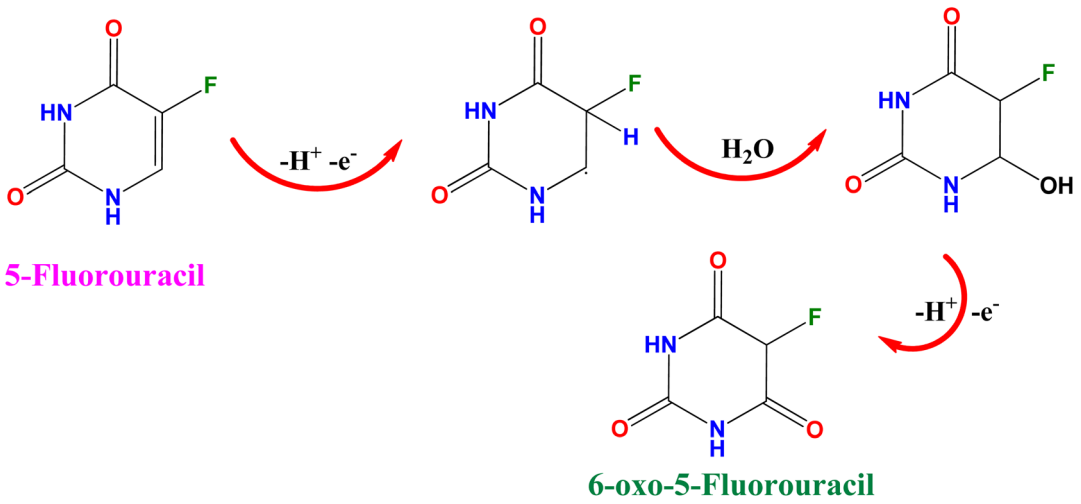

Scheme 4 Electrochemical oxidation of 5-fluorouracil.

active sites, which further accelerates the electrochemical reaction, resulting in higher sensitivity.[64] As shown in Fig. 4(B), the CV technique was conducted across the PTh/h-BN/GCE at varied 5-Fu concentrations (10–150 μM) in 0.1 M PBS (pH 7.0) at a uniform scan rate of 50 mV s^{-1}. When the concentration of 5-Fu rises from 10–150 μM, the peak current response gradually increases due to the PTh/h-BN/GCE has an amount of active surface area available for diffusion and has a higher concentration gradient compared with individual materials of PTh/GCE, and h-BN/GCE. Fig. 4(B) (inset) results illustrate I_{pa} (μA) $= -0.2625x + 22.919$ and the regression coefficient is 0.9839. These outcomes strongly confirm the good electrocatalytic activity of PTh/h-BN/GCE towards the response of 5-Fu.

3.5. Effect of scan rate

To understand the electrocatalytic kinetic behaviour such as oxidation peak potential and peak current of PTh/h-BN/GCE in the presence of 50 μM of 5-Fu in 0.1 M PBS (pH = 7.0), CV were performed for different scan rates from 10 to 200 mV s^{-1} using PTh/h-BN/GCE as a working electrode. Thereby, an increase in scan rate also increases the current response as shown in Fig. 5(A). Moreover, if the scan rate increases linearly, the peak current response moderately changed to the right due to the charge separation of the molecule and mass transfer process on the PTh/h-BN/GCE. This indicates the oxidation of 5-Fu is an irreversible diffusion-controlled process. Furthermore, the important factor of the scan rate study is, both reversible and irreversible systems have the property, that the current peak is proportional to the square root of the scan rate.[65] Fig. 5(A) (inset), shows an excellent linear plot between the 5-Fu current response and the scan rate in mV s^{-1} with a regression coefficient of 0.9518. I_{pa} (μA) $= -0.156$ (mV s^{-1}) $- 33.01$ is the linear regression equation, and this finding implies that the reaction kinetics of PTh/h-BN/GCE electrodes was a surface-controlled process.

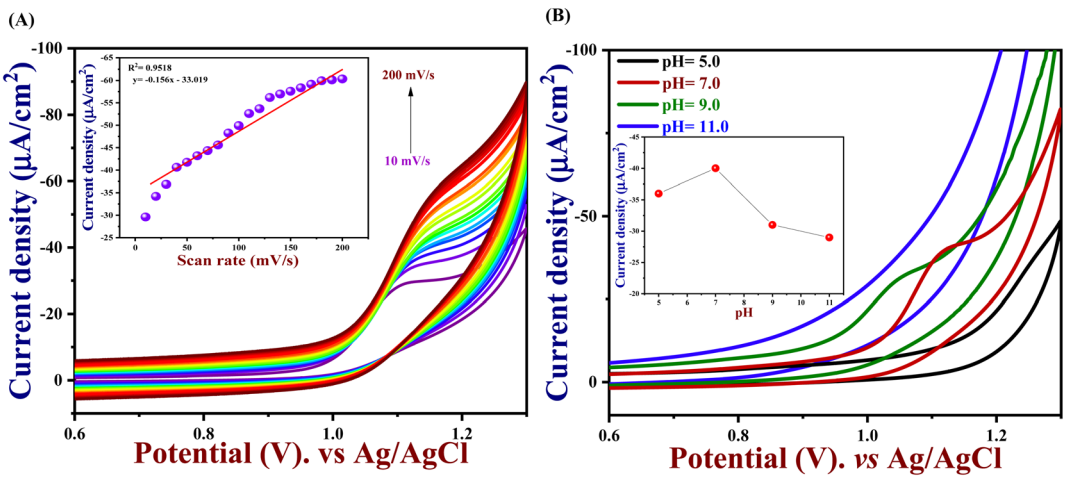

Fig. 5 (A) CV profiles of PTh/h-BN/GCE in 0.1 M PBS (pH 7.0) in 50 μM (5-Fu) with varying scan rates ranging from 10–200 mV s^{-1} (inset: calibration plot of current density *vs.* scan rate), (B) CV profiles of PTh/h-BN/GCE in various pH ranges from 5.0 to 11.0 in (0.1 M PBS) in 50 μM of 5-Fu.

$$E_{pa} = E^{\circ} + \left(\frac{RT}{\alpha nF}\right)\ln\left(\frac{RTk}{\alpha nF}\right) + \left(\frac{RT}{\alpha nF}\right)\ln \nu \quad (3)$$

The Laviron equation, 'E_{pa}', and ln 'ν' connection was used to compute the number of transferred electrons during the irreversible oxidation of 5-Fu (eqn (3)). Because p oxidation is an irreversible process, the coefficient of charge transfer was set to 0.5. Thus, the value of n was determined as 1, indicating that two electrons took part in the electro-oxidation of PTh/h-BN/GCE.

3.6. Effect of pH

In electrochemistry, pH can influence the rates of electrochemical reaction steps by magnitude orders.[66] In this study, the pH was optimized by different pH ranges of 5.0, 7.0, 9.0, and 11.0 towards the detection of 5-Fu investigated at PTh/h-BN/GCE in the presence of 5-Fu at 50 mV s^{-1}. For the oxidation peak of 5-Fu was impacted by the buffer solution's pH. Fig. 5(B), we found that the pH of 7.0 has the highest peak current obtained compared to other pH ranges of 5.0, 9.0, and 11.0, indicating the non-dissociated of 5-Fu in pH 7.0 which possibly gets adsorbed on the surface of GCE. When the pH is increased in the range of 5.0–7.0, the electrochemical signals are amplified, however, the current response decreases when the pH is raised further. This is caused by the development of 5-Fu deprotonation and additionally, it was noted that the peak potential of 5-Fu altered to fewer positive values with increasing the pH of the solution, suggesting that the protons participate in the anodic reaction. The scientific relationship between pH and E_{pa} can be explained using the Nernst equation below (eqn (4)).

$$E_{pa} = E^{\circ} + \frac{0.0591}{n}\log\left[\frac{(OX)^{a}}{(R)^{b}}\right] - \left(\frac{0.0591m}{n}\right)pH \quad (4)$$

where 'a' and 'b' stands for the oxidant and reductant coefficients, 'm' stands for the number of proton participants in the electrochemical reaction, and 'n' stands for the number of electron participants. In this instance, the estimated slope value was 0.0527 V, suggesting that the same number of protons and electrons were involved in the oxidation of 5-Fu.

3.7. Effect of catalyst loading

By applying different amounts of PTh/h-BN nanocomposite dispersion to the GCE surface, the optimum loading of the material for effective 5-Fu oxidation was determined as shown in Fig. S_4.† For these purposes, GCE was modified with varying PTh/h-BN dispersion volumes, as indicated by 4 μL, 6 μL, 8 μL, and 10 μL. By using CV voltammetry, GCE was modified with an amount of 4 μL to 10 μL PTh/h-BN dispersion in the presence of same concentration of 5-Fu. While the dispersion of 8 μL observes a greater catalytic current. However, increasing the catalyst dispersion volume above 8 μL affect the catalytic curve of 5-Fu due to the depth of the PTh/h-BN dispersion. This investigation determined that the optimal catalyst loading was 8 μL of PTh/h-BN on the GCE surface is suitable for the higher sensitivity of 5-Fu.

3.8. Analytical performance of PTh/h-BN for 5-fu detection

DPV method. The mechanism, kinetics, and thermodynamics of chemical reactions are studied using differential pulse voltammetry (DPV), which is also utilized for quantitative chemical analysis.[67] For a quantitative study of 5-Fu, differential pulse voltammetry analysis was recorded with PTh/h-BN/GCE electrode at an applied potential of +1.05 V in the presence of increasing concentration ranges of 5-Fu from 1.0 μM to 360 μM in 0.1 M PBS (pH = 7.0) under the acquired optimum parameters to demonstrate the practical applicability of the developed sensor. It has been determined that 100 mV pulse amplitude, 100 ms pulse width, and 10 mV step increment are the ideal experimental criteria for a good voltammetry profile with a high peak current and minimum background current. We noticed during the DPV investigation, with each addition of 5-Fu, the

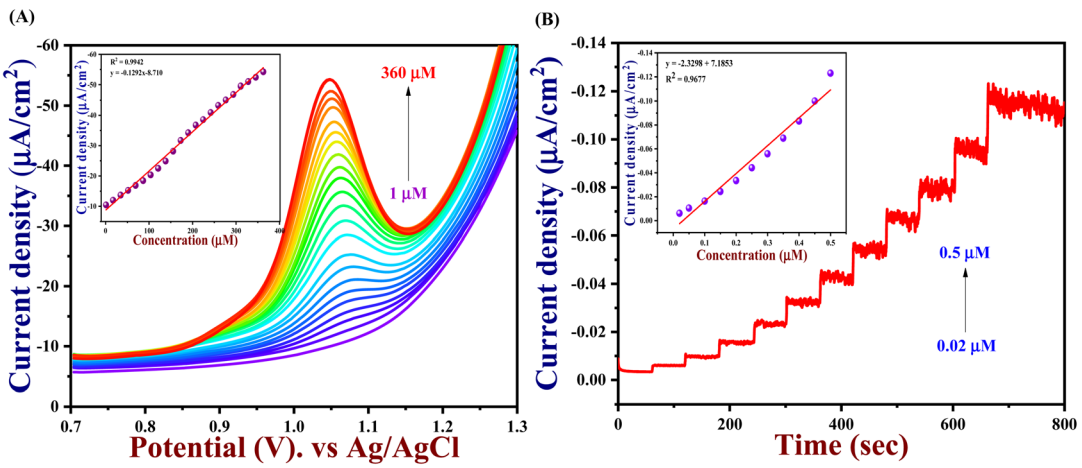

Fig. 6 (A) The DPV response of the fabricated PTh/h-BN/GCE in 0.1 M PBS with the addition of 5-Fu concentration from 1 to 360 μM (inset: calibration plot of current density *vs.* concentration of 5-Fu), (B) the amperometry response of the fabricated PTh/h-BN/GCE in 0.1 M PBS with the addition of 5-Fu concentration from 0.02 to 0.5 μM (inset: calibration plot of current density *vs.* concentration of 5-Fu).

anodic current response linearly increases. According to them, the findings are displayed in Fig. 6(A). At +1.05 V, a clearly defined anodic peak was seen and the peak appearance observed in DPV tests is significantly influenced by the kinetics of electron transport. However, the 5-Fu anodic peak currents improved as the 5-Fu dosage increased and its anodic peak current was found to have a strong linear relationship. Fig. 6(A) (Inset), shows a calibration graph for 5-Fu between I_{pa} and 5-Fu concentrations using the following equation of $I_{pa} = -0.129x - 8.710$ and displays a linear curve with a regression coefficient of 0.9942, '*m*' is the slope value of the linear graph and the LOD was found to be 0.02 μM.

Amperometry method. The amperometry method is a well-known technique that has convective mass transport and can detect 5-Fu rapidly. In comparison to other detection methods, it is more sensitive to evaluate the analyte in sensing applications.[68] Hence, the sensitivity and a lower signal-to-noise ratio are important factors for these applications, and the majority of amperometry sensors were employed by closely monitoring the current variations seen during amperometry excitations. PTh/h-BN/GCE is used as the working electrode in an amperometry (*i–t*) curve for the response of 5-Fu in 0.1 M PBS at a fixed potential of +1.05 V. However, by increasing the concentration of 5-Fu from 0.02 μM to 0.5 μM at a time over a period of 60 s as shown in Fig. 6(B). It demonstrated the PTh/h-BN/GCE's great sensitivity to 5-Fu oxidation at + 1.05 V in 0.1 M PBS (pH 7.0) into a continuous stirring with a rotation speed of 1100 rpm. Although, it revealed that PTh/BN/GCE responded to each addition of 5-Fu with a quick amperometry response, indicating that the electrode and electrolyte interface had a rapid electron transfer mechanism during the 5-Fu addition.

Hence, the current is calculated in amperometry as a function of time or electrode potential and this type of variable is independent. With a correlation value R^2 of 0.9677 with I_{pa} (μA) $= -2.329x + 7.1863$, the linear range for 5-Fu oxidation from concentrations of 0.02 μM to 1 μM was reached is seen in Fig. 6(B) (inset). Finally, the LOD and linear range of the PTh/h-BN modified GCE of analytical parameters have been compared to earlier reported articles and other reported 2D materials towards 5-Fu listed in Table 2.

The *in situ* synthesized nanocomposites with enormous surface areas and more effective sites, the synergistic result between the PTh and the h-BN nanosheets, and the powerful combination between PTh and h-BN are some of the factors that provide the enlarged electro-catalytic activity of the PTh/h-BN-modified GCE to recognize the 5-Fu. These factors can provide a sufficient electrode/electrolyte interaction. These outcomes suggest that the PTh/h-BN hybrid is a potential platform for the sensing of 5-Fu. The following equation was used to determine the limit of detection (LOD) is 3 × S.D./slope. It showed that, in comparison with some of the published 5-Fu sensors, the PTh/h-BN/GCE had shown a good LOD of 0.007 μM and a good linear range of 5-Fu detection.

3.9. Selectivity, reproducibility, repeatability, and stability

An important analytical factor in an electrochemical sensor is the practical analysis of its anti-interference capability. However, the impact of additional electroactive species is frequently attained at an applied working potential under physiological conditions. In real-world applications, it is crucial to assess the selectivity of the 5-Fu sensor since various inorganic compounds may co-exist, and physiologically active molecules may prevent the detection of 5-Fu. Accordingly, the interference study is performed in the DPV and amperometry technique shown in Fig. 7(A) and (B) which the PTh/h-BN/GCE were evaluated at +1.05 V in the presence of 5-fluorouracil and various common interfering molecules, L-ascorbic acid, glucose, L-cystine, lactose, oxalic acid, uric acid, Mg^{2+}, Na^{+}, K^{+} and Ca^{2+} for every 30 seconds to check if any ions are interfering our analyte. Likewise, the sensor response barely changed by around 5% whereas the 5-Fu oxidation current response is not greatly impacted. Due to the sensor's great selectivity towards 5-Fu detection, the interferent molecules failed to generate any appreciable current signals. Moreover, these results suggest the selectivity of the PTh/h-BN hybrid layer-modified electrode was unaffected by the most prevalent interferent molecules. As

Table 2 Comparison of the previously reported sensor with PTh/h-BN/GCE sensor to the detection of 5-Fu

S. no.	Electrodes	Techniques	LOD/μM	Linear range (μM)	Reference
1	Poly(bromocresol purple); double-strand DNA	CV DPV	1.17	32.29–189.96	69
2	PANI nanotube@AgNPs	CV DPV	0.06	1.0–300	12
3	PNIPAM–PEDOT/GC	DPV	0.015	0.03–182	10
4	AuNPs–porphyrin	CV DPV	0.66	29.9–234.4	7
5	N-CQD@Fe_2O_3/MWCNT/GCE	DPV	0.019	0.5–120	70
6	α-Sm_2S_3/MoS_2	CV DPV	0.01	0.1–1166	71
7	Au–MWCNT–chitosan	CV DPV	0.02	0.03–10	72
8	MWNTs/BTB/GCE	DPV	0.2	0.8–5000	15
9	PTh/h-BN/GCE	DPV *i–t*	0.02 0.007	1.0–360 0.02–0.5	This work

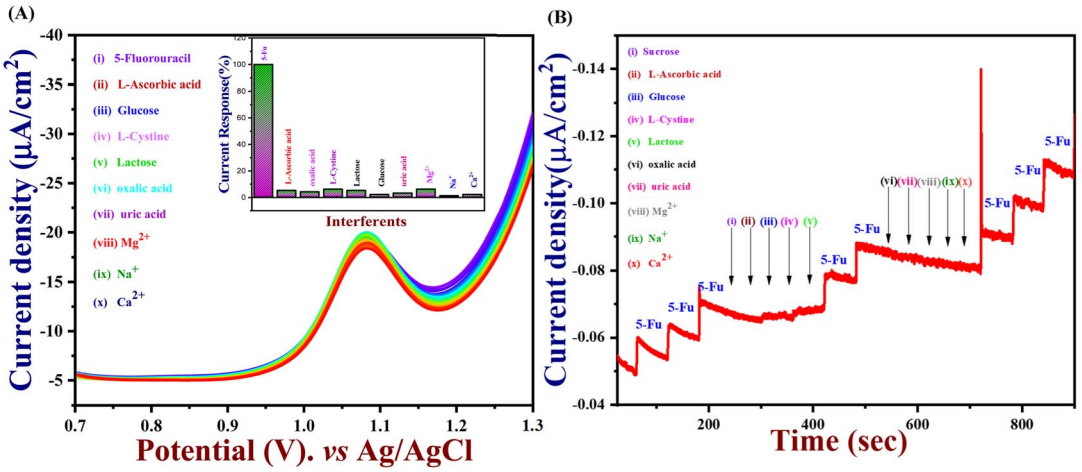

Fig. 7 (A) Selectivity of the PTh/h-BN/GCE with the addition of the same concentration of the interference molecules by DPV techniques (inset: histogram of current response *vs.* various interferent ions), (B) selectivity of the PTh/h-BN/GCE with the addition of the same concentration of the interference molecules by the amperometry technique.

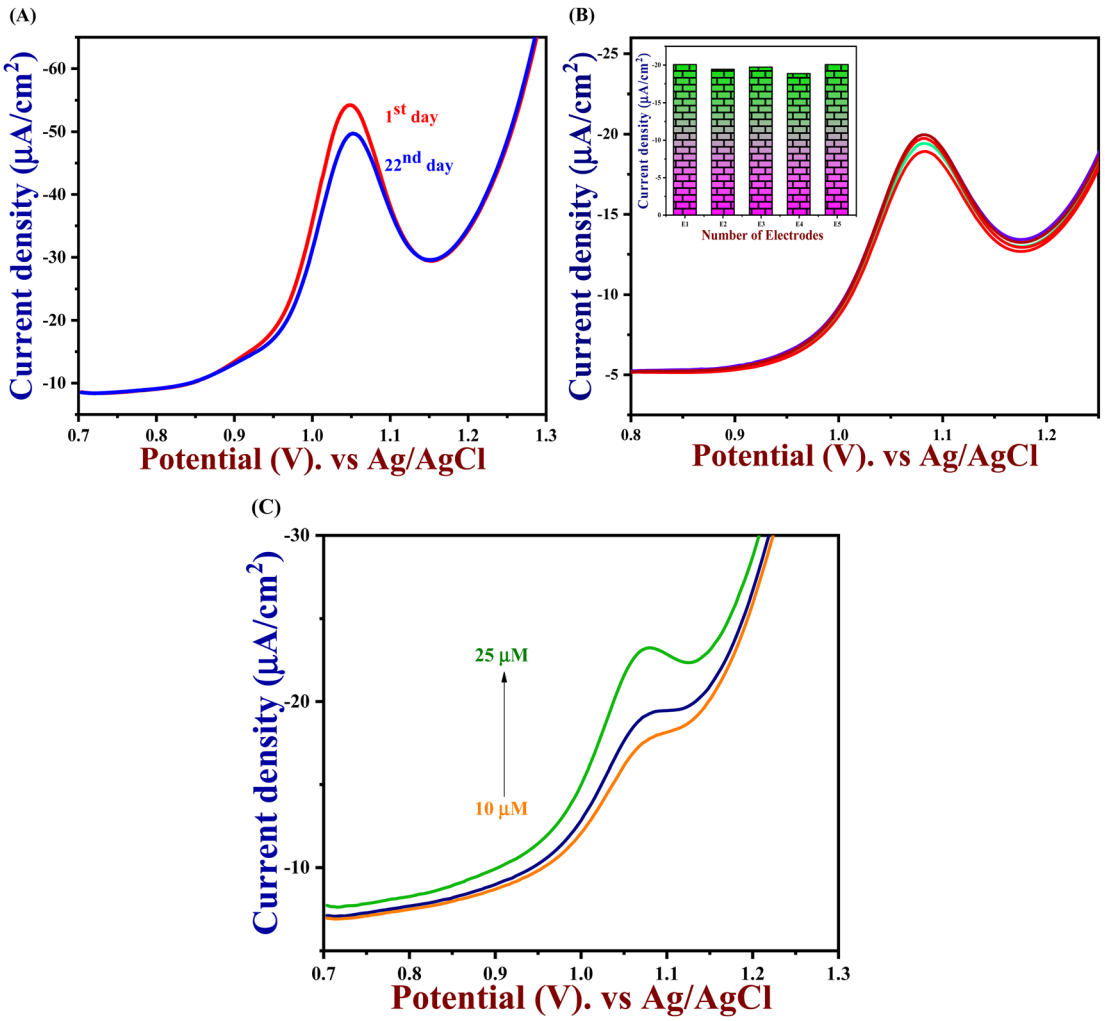

Fig. 8 (A) DPV of PTh/h-BN/GCE in 0.1 M PBS (pH = 7.0) containing 5-Fu with different storage times, (B) DPV of PTh/h-BN/GCE in 0.1 M PBS (pH = 7.0) containing 5-Fu with different modified electrodes (inset: histogram of current density *vs.* number of different modified electrodes). (C) The real sample analysis of 5-Fu at PTh/h-BN/GCE in blood serum in 0.1 M PBS (pH = 7.0).

a result, the presence of co-interfering molecules can function as a selective electrochemical sensor for the anticancer drug of 5-Fu.

The DPV study was used to evaluate reproducibility, repeatability, and long-term durability. To access the repeatability of the sensors, the PTh/h-BN/GCE electrode was made separately and after storing this modified electrode for 21 days, the sensor repeatability was checked and more than 90% of the response was preserved by the sensors seen in Fig. 8(A). This study shows that our material is having a very excellent repeatability. Moreover, the stability study is performed in cyclic voltammetry in the presence of 5-Fu with PTh/h-BN/GCE to check the stability of the composite. Due to the frequent occurrence of electrode fouling with typical solid electrodes employed for the oxidation of 5-Fu, this has great importance. Here, our proposed PTh/h-BN/GCE shows excellent stability after several continue segments of CV responses seen in Fig. S_5.† Furthermore, the reproducibility study is performed in DPV with the five different modified electrodes used to analyze the 5-Fu and there is only a significant current change occurs in the DPV analysis of the five modified electrodes seen in Fig. 8(B). These electrodes show a good reproducibility response towards 5-Fu to conclude our material has excellent reproducibility. Fig. S_6(A)† shows the histogram of current response *vs.* various interferent ions in the presence of target analyte (5-Fu), (B) current density *vs.* of several different electrodes, and (C) current density *vs.* several different modified electrodes.

3.10. Real sample analysis

A blood sample was taken from SRM hospital to assess the PTh/h-BN sensor's dependability for detecting 5-Fu in real samples. After being filtered to remove insoluble impurities, the sample of blood serum was obtained and used for the real sample analysis. Further, the acquired samples of blood were treated with 0.1 M PBS and then used immediately for the DPV analysis under optimal conditions using the conventional addition procedure. While, by analyzing the blood serum sample with various spiked concentrations of 5-Fu (10, 15, and 25 μM), the sensor's applicability was ascertained shown in Fig. 8(C) and Table 3 provide a summary of the outcomes. Moreover, these findings indicated that the proposed sensor performed exceptionally well, with a good recovery rate. Hence, these findings show that the newly suggested PTh/h-BN sensor can successfully detect the 5-Fu in a real sample. Further, its evidence that the suggested method for the identification of 5-Fu was successful comes from the good recoveries for the spiked samples and the absence of any discernible influence from other chemical molecules.

Table 3 Determination of 5-Fu in human blood serum sample using the PTh/h-BN nanocomposite modified GCE

Sl. no.	Sample	Added (μM)	Found (μM)	Recovery (%)
1	Blood sample 1 + spiked	10	9.9	99.8
2	Blood sample 2 + spiked	15	14.8	99.6
3	Blood sample 3 + spiked	25	24.7	99.7

4. Conclusion

In this study, we prepared the PTh/h-BN composite using a straightforward *in situ* Polymerization process toward the detection of 5-Fu. Different methods, including XRD, FT-IR, FE-SEM, and HR-TEM were used to characterize the PTh, h-BN, and PTh/h-BN materials. The % crystallinity of PTh/h-BN is 60.1% and the crystalline size is 3.95 nm. In the voltammetry techniques of CV, DPV, and AMP methods showed that the PTh/h-BN demonstrated a good response to detect an anticancer of 5-Fu. When thiophene was polymerized on the h-BN nanosheets, a composite was formed that made it easier for charge carriers to move along the polymer chains, which significantly enhanced the composite's charge transfer. For the first time, we reported an amperometry method to use for detecting a 5-Fu up to nanomolar level. Additionally, our proposed sensor showed a lower LOD value, excellent linear range, good reproducibility, and better stability for detecting an anticancer drug of 5-Fu. To conclude, the real sample analysis using our suggested sensor yielded positive recovery results. Therefore, the newly proposed sensor material we have is a promising one for the sensor industry.

Author contributions

MM – conceptualization, formal analysis, methodology, experimental operation, validation, data curation, writing – original draft. MG – data curation, writing review, and editing – original draft. BR – review & editing. JAS – funding acquisition, investigation, supervision, visualization, correcting/editing – original draft.

Conflicts of interest

The authors declare no conflict of interest.

Acknowledgements

The authors acknowledge the financial support from the Department of Chemistry, SRM Institute of Science and Technology, Kattankulathur-603203, Tamil Nadu, India. We acknowledge SCIF and the Nanotechnology Research Centre (NRC), SRMIST, for providing the instrumentation facilities.

References

1 C. Wang, L. Shen and L. Wu, *Comput. Methods Biomech. Biomed. Eng.*, 2021, **24**, 151–160.
2 A. S. Ochoa-Chavez, A. Pieczyńska, A. Fiszka Borzyszkowska, P. J. Espinoza-Montero and E. M. Siedlecka, *Chemosphere*, 2018, **201**, 816–825.
3 O. Y. Golubeva, Y. A. Alikina, E. Y. Brazovskaya and V. V. Ugolkov, *Appl. Clay Sci.*, 2020, **184**, 105401.

4 C. Lestuzzi, E. Vaccher, R. Talamini, A. Lleshi, N. Meneguzzo, E. Viel, S. Scalone, L. Tartuferi, A. Buonadonna, L. Ejiofor and H. J. Schmoll, *Ann. Oncol.*, 2014, **25**, 1059–1064.
5 A. Hosseinian, E. Vessally, S. Yahyaei, L. Edjlali and A. Bekhradnia, *J. Cluster Sci.*, 2017, **28**, 2681–2692.
6 D. Basak, S. Arrighi, Y. Darwiche and S. Deb, *Life*, 2021, **12**(1), 48–70.
7 D. Lima, G. N. Calaça, A. G. Viana and C. A. Pessôa, *Appl. Surf. Sci.*, 2018, **427**, 742–753.
8 M. Ali, M. Ijaz, M. Ikram, A. Ul-Hamid, M. Avais and A. A. Anjum, *Nanoscale Res. Lett.*, 2021, **16**, 148.
9 B. C. Grogan, J. B. Parker, A. F. Guminski and J. T. Stivers, *Biochemistry*, 2011, **50**, 618–627.
10 B. Mutharani, P. Ranganathan and S.-M. Chen, *Sens. Actuators, B*, 2020, **304**, 127361.
11 M. D. Wyatt and D. M. Wilson 3rd, *Cell. Mol. Life Sci.*, 2009, **66**, 788–799.
12 F. M. Zahed, B. Hatamluyi, F. Lorestani and Z. Es'haghi, *J. Pharm. Biomed. Anal.*, 2018, **161**, 12–19.
13 R. Sabourian, S. Z. Mirjalili, N. Namini, F. Chavoshy, M. Hajimahmoodi and M. Safavi, *Anal. Biochem.*, 2020, **610**, 113891.
14 X. Jiang, D.-Q. Feng, G. Liu, D. Fan and W. Wang, *Sens. Actuators, B*, 2016, **232**, 276–282.
15 X. Hua, X. Hou, X. Gong and G. Shen, *Anal. Methods*, 2013, **5**, 2470–2476.
16 N. El-Kousy and L. I. Bebawy, *J. Pharm. Biomed. Anal.*, 1999, **20**, 671–679.
17 U. R. Tjaden and E. A. De Bruijn, *J. Chromatogr. B: Biomed. Sci. Appl.*, 1990, **531**, 235–294.
18 F. R. Simões and M. G. Xavier, in *Nanoscience and its applications*, ed. A. L. Da Róz, M. Ferreira, F. de Lima Leite and O. N. Oliveira, William Andrew Publishing, 2017, DOI: 10.1016/B978-0-323-49780-0.00006-5, pp. 155–178.
19 Z. Haghparas, Z. Kordrostami, M. Sorouri, M. Rajabzadeh and R. Khalifeh, *Sci. Rep.*, 2021, **11**, 344.
20 C.-H. Su, C.-L. Sun and Y.-C. Liao, *ACS Omega*, 2017, **2**, 4245–4252.
21 Q. Wang, X. Zhang, X. Chai, T. Wang, T. Cao, Y. Li, L. Zhang, F. Fan, Y. Fu and W. Qi, *ACS Appl. Nano Mater.*, 2021, **4**, 6103–6110.
22 L. Zhao, J. Blackburn and C. L. Brosseau, *Anal. Chem.*, 2015, **87**, 441–447.
23 C. S. Kushwaha and S. K. Shukla, *ACS Appl. Polym. Mater.*, 2020, **2**, 2252–2259.
24 S. Chelly, M. Chelly, R. Zribi, R. Gdoura, H. Bouaziz-Ketata and G. Neri, *ACS Omega*, 2021, **6**, 23666–23675.
25 M. Sakthivel, R. Sukanya, S.-M. Chen and K.-C. Ho, *ACS Appl. Mater. Interfaces*, 2018, **10**, 29712–29723.
26 A. Shah, *ACS Omega*, 2020, **5**, 6187–6193.
27 J. Hu and Z. Zhang, *Nanomaterials*, 2020, **10**(10), 1–14.
28 M. Zamani, J. M. Robson, A. Fan, M. S. Bono, A. L. Furst and C. M. Klapperich, *ACS Cent. Sci.*, 2021, **7**, 963–972.
29 R. Ding, Y. H. Cheong, A. Ahamed and G. Lisak, *Anal. Chem.*, 2021, **93**, 1880–1888.
30 M. Labib, E. H. Sargent and S. O. Kelley, *Chem. Rev.*, 2016, **116**, 9001–9090.
31 M. Tomy, A. Ambika Rajappan, V. Vm and X. Thankappan Suryabai, *Energy Fuels*, 2021, **35**, 19881–19900.
32 Y. Chen, K. Yang, B. Jiang, J. Li, M. Zeng and L. Fu, *J. Mater. Chem. A*, 2017, **5**, 8187–8208.
33 A. Jain, Z. Wang and J. K. Nørskov, *ACS Energy Lett.*, 2019, **4**, 1410–1411.
34 A. Ostadhossein, J. Guo, F. Simeski and M. Ihme, *Commun. Chem.*, 2019, **2**, 95.
35 S. Noreen, M. B. Tahir, A. Hussain, T. Nawaz, J. U. Rehman, A. Dahshan, M. Alzaid and H. Alrobei, *Int. J. Hydrogen Energy*, 2022, **47**, 1371–1389.
36 A. Bolotsky, D. Butler, C. Dong, K. Gerace, N. R. Glavin, C. Muratore, J. A. Robinson and A. Ebrahimi, *ACS Nano*, 2019, **13**, 9781–9810.
37 K. Zhang, Y. Feng, F. Wang, Z. Yang and J. Wang, *J. Mater. Chem. C*, 2017, **5**, 11992–12022.
38 S. Roy, X. Zhang, A. B. Puthirath, A. Meiyazhagan, S. Bhattacharyya, M. M. Rahman, G. Babu, S. Susarla, S. K. Saju, M. K. Tran, L. M. Sassi, M. A. S. R. Saadi, J. Lai, O. Sahin, S. M. Sajadi, B. Dharmarajan, D. Salpekar, N. Chakingal, A. Baburaj, X. Shuai, A. Adumbumkulath, K. A. Miller, J. M. Gayle, A. Ajnsztajn, T. Prasankumar, V. V. J. Harikrishnan, V. Ojha, H. Kannan, A. Z. Khater, Z. Zhu, S. A. Iyengar, P. A. d. S. Autreto, E. F. Oliveira, G. Gao, A. G. Birdwell, M. R. Neupane, T. G. Ivanov, J. Taha-Tijerina, R. M. Yadav, S. Arepalli, R. Vajtai and P. M. Ajayan, *Adv. Mater.*, 2021, **33**, 2101589.
39 R.-E. Munteanu, P. S. Moreno, M. Bramini and S. Gáspár, *Anal. Bioanal. Chem.*, 2021, **413**, 701–725.
40 Z. Meng, R. M. Stolz, L. Mendecki and K. A. Mirica, *Chem. Rev.*, 2019, **119**, 478–598.
41 S. Paszkiewicz and A. Szymczyk, in *Nanomaterials and Polymer Nanocomposites*, ed. N. Karak, Elsevier, 2019, DOI: 10.1016/B978-0-12-814615-6.00006-0, pp. 177–216.
42 M. Shanmugam, A. Augustin, S. Mohan, B. Honnappa, C. Chuaicham, S. Rajendran, T. K. A. Hoang, K. Sasaki and K. Sekar, *Fuel*, 2022, **325**, 124899.
43 M. Ikram, R. Murray, M. Imran, S. Ali and S. I. Shah, *Mater. Res. Bull.*, 2016, **75**, 35–40.
44 M. Mustajab, M. Ikram, A. Haider, A. Ul-Hamid, W. Nabgan, J. Haider, R. Ghaffar, A. Shahzadi, A. Ghaffar and A. Saeed, *Appl. Nanosci.*, 2022, **12**, 2621–2633.
45 T. P. Kaloni, P. K. Giesbrecht, G. Schreckenbach and M. S. Freund, *Chem. Mater.*, 2017, **29**, 10248–10283.
46 M. Ikram, A. Haider, S. T. Bibi, A. Ul-Hamid, J. Haider, I. Shahzadi, W. Nabgan, S. Moeen, S. Ali, S. Goumri-Said and M. B. Kanoun, *RSC Adv.*, 2022, **12**, 32142–32155.
47 W. Al-Graiti, J. Foroughi, Y. Liu and J. Chen, *ACS Omega*, 2019, **4**, 22169–22177.
48 C. L. Weaver, H. Li, X. Luo and X. T. Cui, *J. Mater. Chem. B*, 2014, **2**, 5209–5219.
49 D. Thanasamy, D. Jesuraj, S. K. Konda kannan and V. Avadhanam, *Polymer*, 2019, **175**, 32–40.
50 B. H. Patil, A. D. Jagadale and C. D. Lokhande, *Synth. Met.*, 2012, **162**, 1400–1405.
51 R. Jerome and A. K. Sundramoorthy, *Anal. Chim. Acta*, 2020, **1132**, 110–120.

52 A. Raza, J. Z. Hassan, M. Ikram, S. Ali, U. Farooq, Q. Khan and M. Maqbool, *Adv. Mater. Interfaces*, 2021, **8**, 2002205.
53 M. H. Najar and K. Majid, *J. Mater. Sci.: Mater. Electron.*, 2013, **24**, 4332–4339.
54 R. Jerome, P. V. Keerthivasan, N. Murugan, N. R. Devi and A. K. Sundramoorthy, *ChemistrySelect*, 2020, **5**, 9111–9118.
55 A. Husain, S. Ahmad and F. Mohammad, *Mater. Today Commun.*, 2019, **20**, 100574.
56 V. Yadav and V. Kulshrestha, *Nanoscale*, 2019, **11**, 12755–12773.
57 B. Yu, W. Xing, W. Guo, S. Qiu, X. Wang, S. Lo and Y. Hu, *J. Mater. Chem. A*, 2016, **4**, 7330–7340.
58 R. Liu and Z. Liu, *Chin. Sci. Bull.*, 2009, **54**, 2028–2032.
59 S. Wang, J. Zhang, O. Gharbi, V. Vivier, M. Gao and M. E. Orazem, *Nat. Rev. Methods Primers*, 2021, **1**, 41.
60 N. O. Laschuk, E. B. Easton and O. V. Zenkina, *RSC Adv.*, 2021, **11**, 27925–27936.
61 A. J. Bard, L. R. Faulkner and H. S. White, *Electrochemical methods: fundamentals and applications*, John Wiley & Sons, 2022.
62 P. Veerakumar, G. Jaysiva, S.-M. Chen and K.-C. Lin, *ACS Appl. Mater. Interfaces*, 2022, **14**, 5908–5920.
63 S. D. Bukkitgar and N. P. Shetti, *Mater. Sci. Eng., C*, 2016, **65**, 262–268.
64 X. Liu, L. Huang and K. Qian, *Adv. NanoBiomed Res.*, 2021, **1**, 2000104.
65 G. Muthukumar, R. Jerome, P. K. Udhaya Ganesh, M. Magesh Kumar, J. Balamurugan and J. Arockia Selvi, *ACS Appl. Nano Mater.*, 2023, DOI: **10.1021/acsanm.2c04322**.
66 M. C. O. Monteiro and M. T. M. Koper, *Curr. Opin. Electrochem.*, 2021, **25**, 100649.
67 B. J. Venton and D. J. DiScenza, in *Electrochemistry for Bioanalysis*, ed. B. Patel, Elsevier, 2020, DOI: **10.1016/B978-0-12-821203-5.00004-X**, pp. 27–50.
68 A. Amine and H. Mohammadi, in *Encyclopedia of Analytical Science*, ed. P. Worsfold, C. Poole, A. Townshend and M. Miró, Academic Press, Oxford, 3rd edn, 2019, DOI: **10.1016/B978-0-12-409547-2.14204-0**, pp. 85–98.
69 D. Koyuncu Zeybek, B. Demir, B. Zeybek and Ş. Pekyardımcı, *Talanta*, 2015, **144**, 793–800.
70 M. Ganesan, K. D. Ramadhass, H.-C. Chuang and G. Gopalakrishnan, *J. Mol. Liq.*, 2021, **331**, 115768.
71 V. Mariyappan, M. Keerthi, S.-M. Chen and G. Boopathy, *J. Electrochem. Soc.*, 2020, **167**, 117506.
72 M. Satyanarayana, K. Y. Goud, K. K. Reddy and K. V. Gobi, *Electrochim. Acta*, 2015, **178**, 608–616.